Nozzles," Final Rept., Aug. 1965, Union Carbide Corp., Tarrytown, N.Y.

[12] Rosner, D. E. and Allendorf, H. D., "Comparative Studies of the Attack of Pyrolytic and Isotropic Graphites by Atomic and Molecular Oxygen at High Temperatures," *AIAA Journal*, Vol. 6, No. 4, April 1968, pp. 650–654.

[13] Walls, J. R. and Strickland-Constable, R. F., "Oxidation of Carbon Between 1000–2400°K," *Carbon*, Vol. 1, 1964, pp. 333–338.

[14] Nagle, J. and Strickland-Constable, R. F., "Oxidation of Carbon Between 1000–2000°C," *Proceedings of the Fifth Carbon Conference*, Vol. I, Pergamon Press, New York, pp. 154–164.

[15] Duval, X., *Journal de Chemie Physique et de Physicochimie Biologique*, Vol. 47, 1950, p. 339.

[16] Walsh, P. N. et al., "Principles Governing the Behavior of Solid Materials in Severe High Temperature Environments," Quarterly Progress Rept. UCRI-326, Sept. 1965, Union Carbide Research Inst., Tarrytown, N. Y.

[17] Walsh, P. N. et al., "Principles Governing the Behavior of Solid Materials in Severe High Temperature Environments," Final Rept. UCRI-388, May 1966, Union Carbide Research Inst., Tarrytown, N.Y.

[18] Walsh, P. N. et al., "Principles Governing the Behavior of Solid Materials in Severe High Temperature Environments," Quarterly Progress Rept. UCRI-353, Dec. 1965, Union Carbide Research Inst., Tarrytown, N.Y.

[19] Bradshaw, W. G., Bonesteel, R. M., and Ong, J. N., "Kinetic Studies on the AGOT and Pyrolytic Graphite," Lockheed Missiles & Space Co. Rept., 1965, Lockheed Missiles & Space Co., Sunnyvale, Calif.

[20] Tesner, P. A., "The Activation Energy of Gaseous Reactions with Solid Carbon," *8th Symposium (International) on Combustion*, Williams and Wilkins, Baltimore, Md., 1962, p. 807.

[21] Essenhigh, R. H., "Discussion of 'The Activation Energy of Gaseous Reactions with Solid Carbon,'" *8th Symposium (International) on Combustion*, Williams and Wilkins, Baltimore, Md., 1962, p. 813.

[22] Lewis, J. C., Floyd, I. J., and Cowlard, F. C., "A Laboratory Investigation of Carbon-Gas Reactions of Relevance to Rocket Nozzle Erosion," *AGARD Conference Proceedings No. 52*, Tech. Edit. and Reproduction, Ltd., London, England, Feb. 1970.

[23] Gulbransen, E. A., Andrew, K. F., and Brassart, F. A., "Reactions of Graphite with CO_2 at 1000–1600°C Under Flow Conditions," *Carbon*, Vol. 2, 1965, pp. 421–429.

[24] Wicke, E., "Contribution to the Combustion Mechanism of Carbon," *5th Symposium (International) on Combustion*, Williams and Wilkins, Baltimore, 1956, pp. 245–252.

[25] Ergun, S., "Panel Discussion—Heterogeneous Burning," *5th Symposium (International) on Combustion*, Williams and Wilkins, Baltimore, Md., 1956, pp. 797–798.

[26] Blakley, J. and Overholser, L., "Oxidation of ATJ Graphite by Low Concentrations of Water Vapor and CO_2 in Helium," *Carbon*, Vol. 3, 1965, pp. 269–275.

[27] Schissel, P. O. and Trulson, O. C., "Mass Spectrometric Study of the Oxidation of Tungsten," *The Journal of Chemical Physics*, Vol. 43, 1965, p. 737.

[28] Batty, J. C. and Stickney, R. E., "Quasi Equilibrium Treatment of Gas-Solid Reactions. I. Evaporation of Volatile Species Formed in the Reaction of O_2 with W, Mo, and C," *The Journal of Chemical Physics*, Vol. 51, 1970, p. 4475.

MAY 1971 J. SPACECRAFT VOL. 8, NO. 5

Influence of Asymmetric Transition on Re-Entry Vehicle Characteristics

A. MARTELLUCCI* AND R. S. NEFF†
General Electric Company, Philadelphia, Pa.

The results of this experimental and analytical study indicate that mass transfer and asymmetric boundary-layer transition strongly influence the motion of a slender re-entry vehicle by changing its static stability characteristics. The angle-of-attack divergence, normally encountered in the transitional altitude regime, can be attributed in whole or in part to the nonlinear behavior of the static forces and moments due to the asymmetries of transition. Mass addition amplifies these forces and moments.

Nomenclature

A_B = model base area
A_S = blowing region surface area
C_A, C_N = axial, normal force coefficients, force/$q_\infty A_B$
C_m = pitching moment coefficient, moment/$q_\infty A_B D_B$
$C_{m_\alpha}, C_{N_\alpha}$ = pitching moment, normal force coefficient slopes at $\alpha = 0°$
D_B, L = model base diameter and length, respectively
$\dot{m}$ = integrated mass addition rate, $\int (\rho v)_w dA_S$
M = Mach number
P, q = pressure and dynamic pressure, respectively
Re_∞ = freestream unit Reynolds number, $\rho_\infty V_\infty/\mu_\infty$
Re = local unit Reynolds number, $\rho_e u_e/\mu_e$
R_B, R_N = base and nose radii, respectively
s = wetted length
SCAAT = sphere cone at angle of attack Program
u, v = velocity components parallel and normal to surface
V_∞ = freestream velocity
VIZAAD = viscous interaction zero angle of attack drag Program
x_{cg} = center of gravity location
$(x/L)_B$ = blowing front location ($\alpha = 0°$)
α = pitch angle of attack
δ = boundary-layer thickness
δ^*, θ = displacement and momentum thicknesses
θ_c = cone half-angle
λ_∞ = blowing coefficient, $(\rho v)_w/(\rho u)_\infty$
μ = viscosity
ρ = mass density

Presented as Paper 70-987 at the AIAA Guidance, Control and Flight Mechanics Conference, Santa Barbara, Calif., August 17–19, 1970; submitted August 24, 1970, revision received March 1, 1971. This work was supported by Contract F04701-69-C-0016 and sponsored by SAMSO and ARPA.

* Consultant, Aerothermodynamics Laboratory, Re-entry and Environmental Systems Division. Associate Fellow AIAA.

† Engineer, Aerothermodynamics Laboratory, Re-entry and Environmental Systems Division. Member AIAA.

Subscripts

e = local boundary-layer edge conditions
L,s = based on length, wetted length, respectively
0 = no mass addition
w, ∞ = wall, freestream conditions
N = based on nose radius

Introduction

MANY phenomena affect the motion of a re-entry vehicle. One particular factor is heat-shield ablation, which depends on the state of the boundary layer. During the period when a transitional boundary-layer exists, the effects of ablation on the motion are substantially more complex.[1-3] In this altitude regime, vehicles generally exhibit a momentary angle-of-attack (α) divergence. Such alterations in motion may be detrimental to the system performance of ballistic and maneuvering re-entry vehicles. This α divergence usually is accompanied by large oscillations in the "effective" pitching moment coefficient slope during transition progression over the surface. It had been postulated that this phenomenon represented dynamic instabilities incurred during transition, but the present studies indicate it can be attributed at least in part to the effects of asymmetric transition on the static stability. Furthermore, the magnitude of the influence is sensitive to the mass addition rate ($\dot{m}$) and distribution, which are affected by the transitional-turbulent heating rates. Consequently, one must re-examine the analyses and coupling mechanisms that led to the earlier conclusions.

In this investigation the transition front shape is experimentally defined as a function of α and Reynolds number Re_∞. Based on these shapes, incremental forces and moments attributable to the asymmetries were measured as a function of α, Re_∞ and $\dot{m}$. The influence of asymmetric transition on the vehicle motion is established by six-degree-of-freedom computer simulations.

Experimental Program

Since ablation is a key parameter that affects vehicle loads, a porous model was used for the force phase of testing. A heat-transfer model was used to define the shape and location of the transition front as a function of α and Re_∞. Although mass addition affects the onset and the shape of the transition front, for the purposes of this investigation (i.e., to establish first-order effects), it was deemed adequate to utilize the impervious model results. The experiments were conducted at the Arnold Engineering Development Center, Tunnel B facility, at a Mach number of 8.

The first phase of the experimental investigation, was to map the transitional flow region of the nonblowing heat-transfer model for each Re_∞ and α. The model was a 7.2° half-angle cone, 43.54 in. long with an interchangeable nose section. It was fabricated of stainless steel with a nominal wall thickness of 0.050 in. Thermocouples were connected to the inner wall of the model for recording the aerodynamic heat transfer. There were 100 thermocouples primarily along five conical rays (ϕ = 0° (lee side), 45°, 90°, 135°, 180°). Several additional thermocouples were installed at $\phi > 180°$ to verify the yaw symmetry of the flow. Data were obtained for ranges of Re_∞ and α so that the end of transition (i.e., the beginning of turbulent flow or the point of maximum heat transfer) would span the model from near the aft end to a point as far forward as possible.

Based upon the foregoing transition front data, force and moment data were next obtained for the simulated ablation case using a 43.3-in.-long, 7.25° half-angle cone, having a porous outer shell manufactured from 90% dense stainless steel-nickel alloy (Fig. 1a). The internal structure was a perforated metal shell which fit snugly to the interior surface of the porous shell (Fig. 1b). Various blowing distributions were obtained by placing a 0.0005-in.-thick aluminized mylar

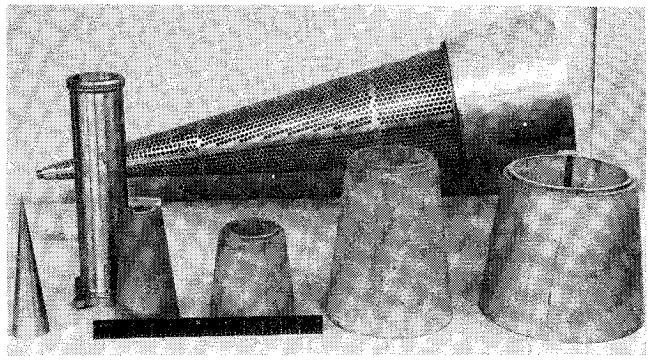

Fig. 1a Photograph of the porous model subcomponents.

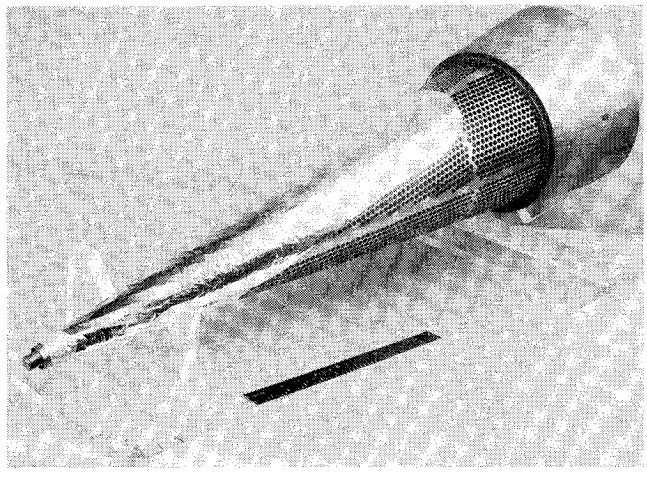

Fig. 1b Photograph of a typical mylar blanket for controlling the mass distribution.

sheet between the perforated shell and the outer porous shell such that the model was impervious over the forward portion (laminar-transitional region) and was porous over the aft portion (turbulent region). Blowing rates, $\lambda_\infty \equiv (\rho v)_w/(\rho u)_\infty$, were varied so as to encompass a range of heat-shield characteristics varying from that for carbon phenolic (small blowing) to that for Teflon (large blowing) (in the local sense, not for integrated values over the vehicle surface). For each Re_∞, data were obtained for three blowing configurations which corresponded to α = 0°, 1°, and 2°; for each configuration λ_∞ was varied from 0 to 0.008.

The blowing or porosity uniformity of the force model was established prior to the test by means of a venturi calibrating device with the external surface of the model at atmospheric conditions. The conical venturi had a 10:1 contraction ratio with a throat area of 0.1 in.^{2} Differential pressures between throat and plenum were recorded with a ±1 psid transducer. Gas samples were obtained by attaching a contoured rubber adapter which was fitted to the cone surface. Readings of local mass flux $(\rho v)_w$ were obtained along four rays of the model which were 90° apart. The calibration indicated that the model porosity was symmetric to within ±25%.

Data Presentation and Analysis

Transition Shape Data

Heat-transfer data defining the shape of the transition front were obtained on the cone along several conical rays. Comparisons of the data obtained at zero angle of attack with the results of the Viscous Interaction Zero Angle of Attack Drag (VIZAAD) Program[4] are shown in Fig. 2. For laminar flow, the heat transfer is calculated from Lee's laminar flow

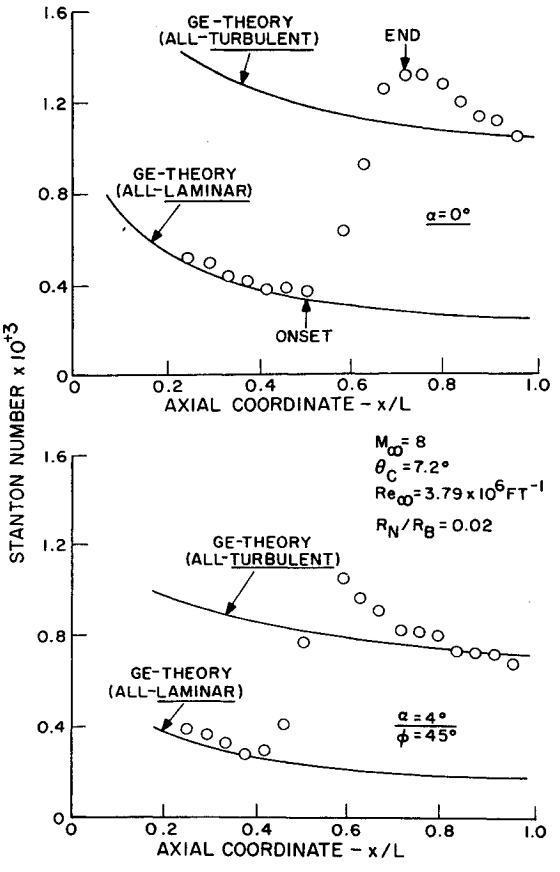

Fig. 2 Heat-transfer distribution on a cone.

equation[5] modified by reference enthalpy conditions to account for the variation of flow properties across the boundary layer. For turbulent flow, Walker[6] obtained a solution for the combined momentum and energy integral equations.

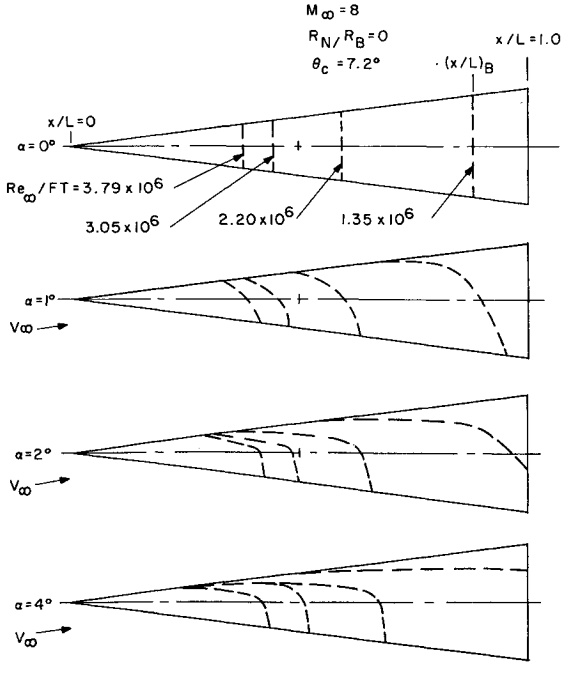

Fig. 3 Spatial distribution of end of transition with Reynolds number and angle of attack $M_\infty = 8$, $R_N/R_B = 0$, $\Theta_c = 7.2°$.

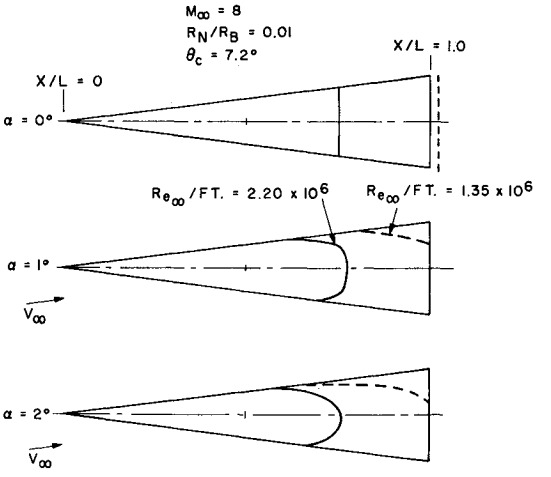

Fig. 4 Spatial distribution of end of transition with Reynolds number and angle of attack, $M_\infty = 8$, $R_N/R_B = 0.01$, $\Theta_c = 7.2°$.

In general, solutions were obtained wherein the state of the boundary layer was either all-laminar or all-turbulent. There is excellent agreement between data and theory in the laminar region. The data exhibit an increase through the transitional flow region to a peak which is higher than the "all-turbulent" theory.‡ The heat transfer then decays at a rate somewhat faster than the "all-turbulent" theory. Theory and data are in good agreement at $\alpha = 0°$ for turbulent flows in the region far removed from the end of transition. Some data comparisons of the angle-of-attack data were made with the results of the Sphere Cone Angle of Attack (SCAAT) program.[7] Shown in Fig. 2, for example, is a comparison for $\alpha = 4°$ for one meridian ray. In general, the data and the SCAAT program results agreed quite well for both laminar and turbulent boundary-layer flows.

Using the data from the first test phase, the location of the transition onset point was defined as the point where the heat transfer (i.e., the Stanton number) is a minimum. The end of transition was deduced to be the point where the heat transfer is a maximum. Since the blowing schedule was tailored to the end of transition location, emphasis was placed on these data. For the sharp cone, the end of transition at angle of attack tends to move slightly rearward from the $\alpha = 0°$ location on the windward ray, and forward on the leeward ray, the latter movement being more pronounced (Fig. 3). This trend is similar to the sharp-cone phenomena observed by others[8-11] and implies that transition occurs at a significantly lower local Re on the lee side than the windward ray. This forward movement on the lee side has classically been attributed to the destabilizing influences of cross flow. As the cone is blunted to a value of $R_N/R_B = 0.01$ ($R_N = 0.055$ in.), the transition point moves forward from the $\alpha = 0°$ point on both the windward and leeward rays (Fig. 4), with greater movement on the lee side. This trend with bluntness is identical to that noted by Stetson and Rushton[9] for bluntness ratios of $R_N/R_B = 0.04$ and 0.08 ($R_N = 0.125$ in. and 0.250 in.). For $R_N/R_B = 0.02$ (Fig. 5), a reversal occurs. Namely, the transition point moves farther forward on the windward ray than on the leeward ray, and the end of transition was farthest aft on the $\phi = 45°$ ray. (Additional experimental details may be found in Ref. 12.)

One can speculate that the apparent transition reversal on the lee side of the model is a result of the coupling of the effects of R_N/R_B and α on transition. Stetson and Rushton[9] conducted a limited investigation of this matter, and the results indicate that transition onset was always further forward

‡ The effective origin approach adequately predicts the magnitude of the "overshoot" in heat transfer.[12]

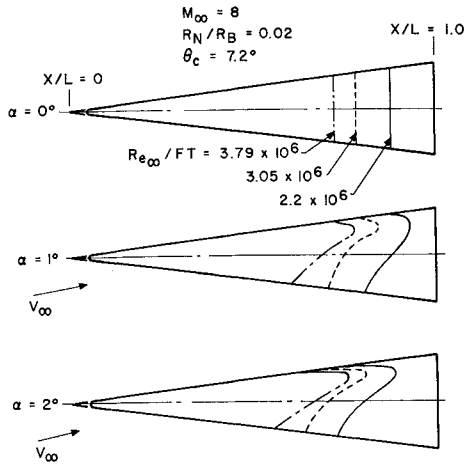

Fig. 5 Spatial distribution of end of transition with Reynolds number and angle of attack, $M_\infty = 8$, $R_N/R_B = 0.02$, $\Theta_c = 7.2°$.

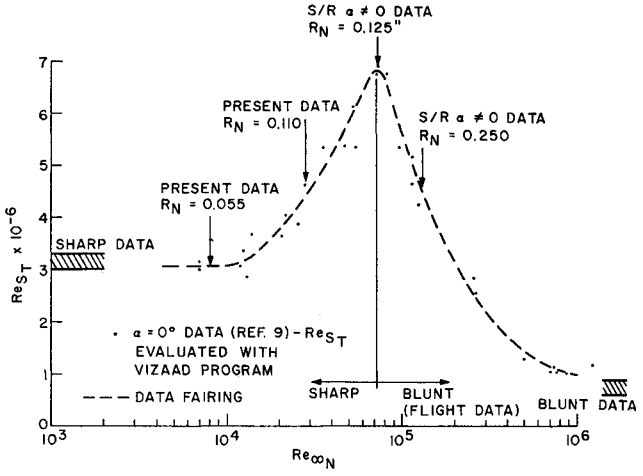

Fig. 6 Local transition Reynolds number variation with bluntness.

on the leeward than on the windward side, in direct agreement with our data for $R_N/R_B = 0$ and 0.01. Available data indicate that bluntness could produce a transition reversal (Fig. 6); i.e., for a prescribed set of freestream conditions, as nose bluntness increases from zero, transition tends to move aft on the vehicle. The aft movement of transition reaches a maximum at some bluntness ($Re_{\infty_N} \approx 8 \times 10^4$) beyond which the transition point moves forward with increasing nose radius. Furthermore, at angle of attack, due to crossflow effects, the bluntness-induced entropy layer is swallowed sooner on the windward ray than on the leeward ray. This implies that for a cone with some finite bluntness, the lee side behaves as if it were more blunt and the windward side less blunt than the comparable $\alpha = 0°$ case. Thus, it follows that the bluntness/angle-of-attack reversal phenomena could occur for cones with a bluntness for which Re_{∞_N} lies slightly to the left of the peak shown in Fig. 6. All the data for either sharp cones or blunted cones with $Re_{\infty_N} > 8 \times 10^4$ indicate that transition lies further forward on the lee side than on the windward side.

Flight test data for ablating and nonablating slender reentry vehicles generally indicate that transition is farther forward on the leeside than on the windward side. Furthermore, most flight test R/V's have nose radii that place them on the blunt side of the transition curve of Fig. 6. Consequently one should expect transition configurations similar to Figs. 3 and 4 to represent flight test trends as opposed to the special case of Fig. 5. At this point, it is appropriate to comment on the current state of prediction capability for boundary-layer transition at $\alpha = 0°$. Approaches currently used to predict the altitude at which transition will occur are empirical correlations based upon the Mach number M_e and wetted-length Reynolds number Re_s at the edge of the boundary layer. Since this approach does not rigorously account for mass addition, surface temperature, and roughness effects (among others), and since the values of M_e and Re_s where transition will occur are not predictable from theory, data from flight tests of vehicles with approximately similar geometry, materials, and re-entry conditions are utilized to establish the criterion. Such correlations generally fail for vehicles other than the generic class for which they were designed. In fact it is evident that not only are there significant differences of opinion within the aerospace community with regard to a suitable transition correlation for the $\alpha = 0°$ case, but also M_e and Re_s are not sufficient to characterize the transition phenomena. Thus, the current state-of-the-art approaches concerning boundary-layer transition prediction are at best marginally adequate for the 2-D (axisymmetric) case and nonexistent for the 3-D ($\alpha \neq 0°$) case.

Force and Moment Data

Since the transition front is forward on the lee side for flight test data, it can be concluded that the sharp-cone data provided transition front shapes that will tend to maximize, for a prescribed α, the incremental moment coefficient ΔC_m due to the skewed front. Force and moment data were obtained with the porous model configured to ablate (i.e., blow) consistent with the 0°, 1°, and 2° transition front shapes that were established in Fig. 3. Measurements were made at Mach 8 for five values of Re_∞ and several values of λ_∞. The α increments were selected to establish not only the incremental forces and moments for the prescribed angle of attack of the blowing front α_F but also the slopes of the coefficients (i.e., C_{N_α} and C_{m_α}). Because of the nonlinear nature of the phenomena, small increments about α_F were selected (i.e., ±0.5°). Furthermore, data were obtained for approximately a 6° spread about each reference angle of attack, α_F.

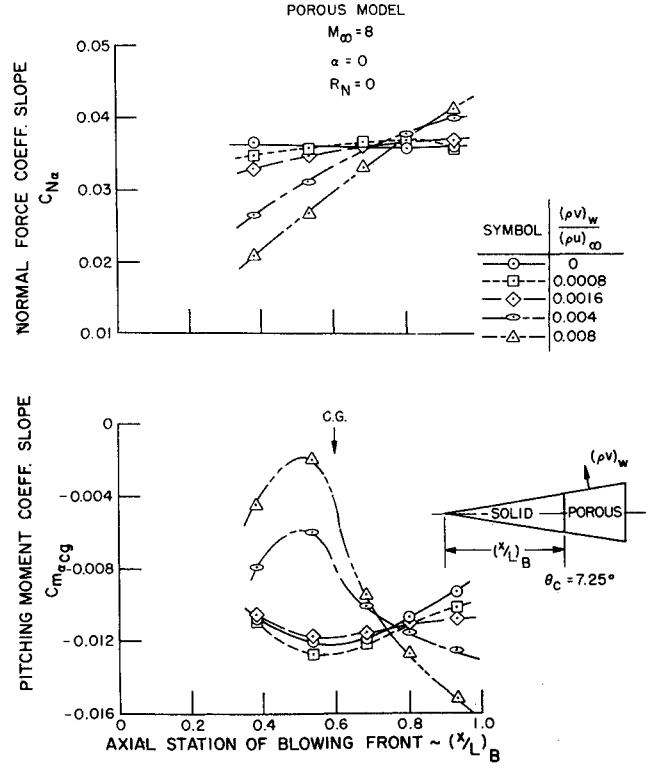

Fig. 7 Effect of transition progression on static stability.

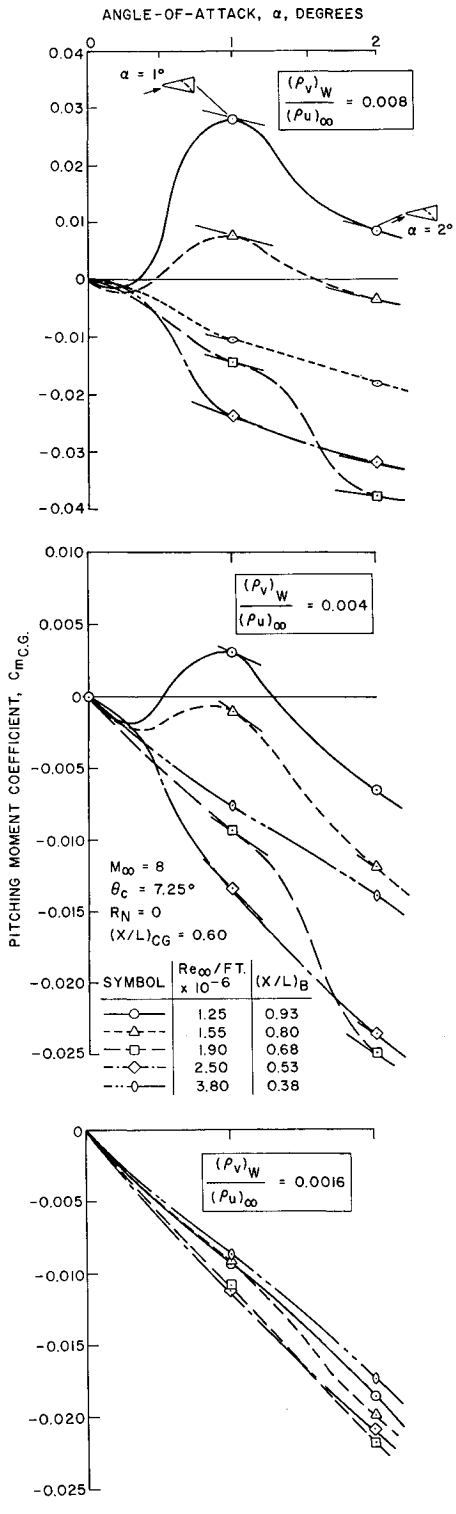

Fig. 8 Pitching moment coefficient variation with angle of attack and blowing configuration.

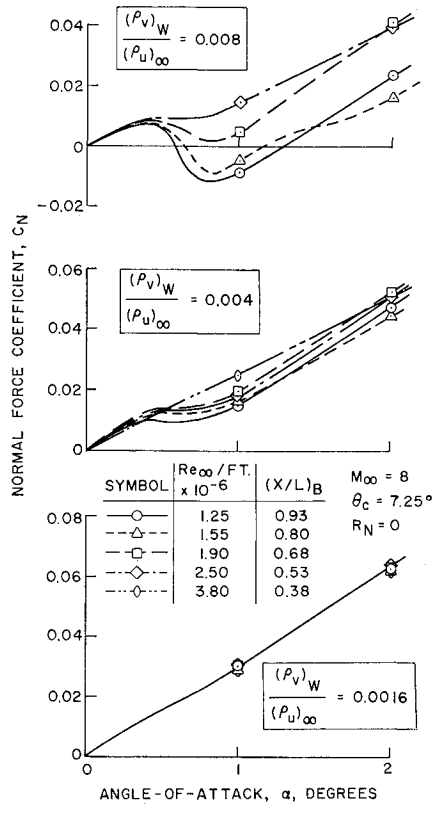

Fig. 9 Normal force coefficient variation with angle of attack and blowing configuration.

Zero Angle of Attack Data

For the axisymmetric configurations, Fig. 7 shows the $\alpha = 0°$ values of $C_{N\alpha}$ and $C_{m\alpha}$ evaluated at $\alpha = 0°$ vs $(x/L)_B$, the blowing front location. These data represent an attempt to match the location of the turbulent front with the increased blowing rate in the turbulent region. For low or zero blowing rates, the static stability increases as the simulated transition region encompasses a greater surface area [$(x/L)_B$ decreasing]. This can be attributed to the greater effective cone angle [$\theta_c + \tan^{-1}(d\delta^*/ds)$] with the more forward location of blowing. For higher blowing rates, the static stability was reduced as the blowing area became greater. Apparently, aerodynamic body shaping, to which base bleed is a contributor, offsets the stability increase due to the effective cone angle. In flight, the distribution of mass addition, which can either be due to nonuniform heat shield materials or to transition movement on a body at $\alpha = 0°$, can have a large effect on the vehicle stability. For example, a vehicle with a high-temperature ablative nose and Teflon over the rear half has roughly one-eighth the stability of an equivalent cone with only the last 10% of its length made of Teflon. This result indicates that for the latter, the equivalent flaring effectiveness due to increased blowing is quite large. As the blowing surface increases, the effectiveness is large but becomes negative, i.e., the stability is less than for the no blowing case, because of the effects of crossflow. It is evident from the data that the motion of small vehicles with low-temperature heat shields would be especially sensitive to what are apparently slight variations in external configuration or heat shield material distribution.

Angle-of-Attack Data

For a re-entering flight vehicle which has asymmetric transitional boundary-layer flow on the surface, the shape of the front and the ensuing higher heating and increased ablation is achieved naturally for a given α. In this ground-test investigation, the shapes which were obtained naturally on the impervious model (i.e., sans trips) were artificially imposed on the porous model. Thus, when the model was manipulated through an α cycle, the blowing front remained fixed, and in this sense does not reflect what occurs in flight. Nevertheless, in the ground test, at select points in the α cycling, proper values of C_N and C_m, and, to a lesser degree, $C_{N\alpha}$ and $C_{m\alpha}$ coefficients were achieved. Particular values of C_N and C_m as a function of α that would correspond to the equivalent flight case were established from the data, as were $C_{N\alpha}$ and $C_{m\alpha}$ at this point.

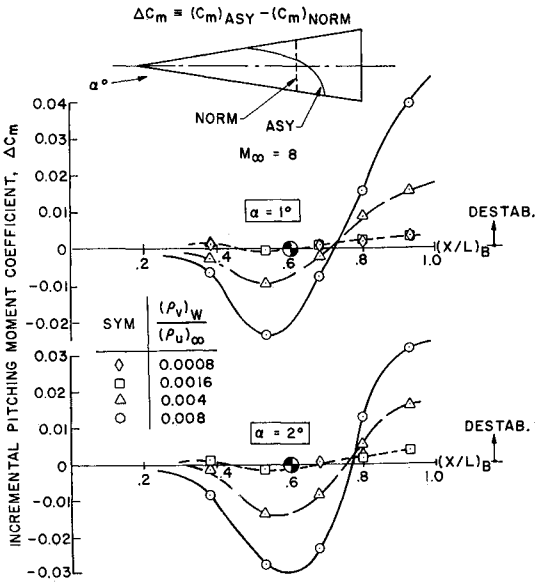

Fig. 10 Incremental pitching moment coefficient due to asymmetric transition.

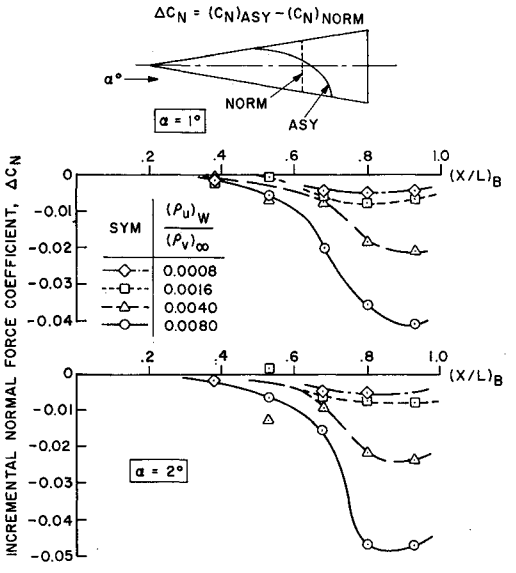

Fig. 11 Incremental normal force coefficient due to asymmetric transition.

Consistent with the above approach, $C_m(\alpha)$ for a cone with the transition front traversing the surface is shown in Fig. 8, and $C_N(\alpha)$ is shown in Fig. 9. Each figure represents a collection of the data for a prescribed blowing rate. It is evident that this is a highly nonlinear phenomenon. For the large blowing rates (λ_∞ = 0.004, 0.008), although the vehicle is stable in the vicinity of $\alpha = 0°$, it is, in fact, statically unstable for $\alpha \gtrsim 0.5°$ when the transition front is on the aft end. Furthermore, mass addition clearly serves as an amplification factor.

The lines faired through the data between $\alpha = 0$ and 1° are questionable due to the paucity of data. However, the question of whether the vehicle is stable or unstable about $\alpha = 0°$ is germain to the data fairing. It is felt by the authors that the vehicle is stable for some small α range, since the destabilizing influences of the asymmetric front must detract from the inherently stable vehicle in some gradual manner.

The incremental values of C_m (Fig. 10) that can be attributed to asymmetric transition were established from:

$$\Delta C_m = (C_m)_{\text{asymmetric}} - (C_m)_{\text{normal}}$$

where $(C_m)_{\text{asymmetric}}$ is defined for particular blowing configuration at its design angle of attack, α_F, and $(C_m)_{\text{normal}}$ corresponds to the C_m that is attained for the axisymmetric blowing configuration for the same Re and α. In a similar way, values of ΔC_N (Fig. 11) were established.

The value of $(x/L)_B$ for which each data point is plotted corresponds to the $\alpha = 0°$ transition location for its value of Re_∞. The presence of the asymmetric transition front at the vehicle aft end initially produces a destabilizing influence. As the front progresses forward (increasing Re_∞ or decreasing altitude), the influence becomes stabilizing. As the front progresses farther forward, the stabilizing influence decreases and in fact becomes slightly destabilizing. This figure bears a striking similarity to flight data curves of stability variation with altitude during transition. From Fig. 11 one observes that ΔC_N is such that it produces a smaller value of C_N, although ΔC_m changes sign at least twice; this implies that the center of pressure is rapidly changing with front location. Furthermore, it is rather evident from these figures that mass addition induces large pressures on the cone surface and therefore acts as a load amplification factor.

Vehicle Motion Implications

The question that arises now is this: Can the rather large variations in static stability due to asymmetric transition, in themselves, affect the vehicle motion? In answering this question one must be careful not to use linear aerodynamic analyses, for the rather obvious reasons stated previously.

In the flight test motion simulations that have customarily been performed, variations of the aerodynamic coefficient were established from theoretical analyses and/or ground test data for "aerodynamically" axisymmetric configurations. The variation of C_N and C_m that result are well-behaved functions which slowly vary with altitude. The dynamic stability parameter used in these simulations is obtained from an iterative solution of the motion simulations. What results is a variation of the dynamic stability parameter with altitude for which the vehicle motion is duplicated. From analyses such as these, one generally finds that a small period of dynamic instability is required to match the measured flight motions. This leads to the much used phrase "dynamic instabilities during transitional flow cause the angle-of-attack divergence". In essence, what is accomplished by this technique is to incorporate into the dynamic parameter all of the uncertainties associated with transitional flow. As stated earlier, one must ask, "Is there another physical phenomenon which could cause similar vehicle motions either independently or acting in concert with the dynamic stability?"

In this investigation, this phenomenon is assumed to be the incremental static forces and moments that can be caused by asymmetric transition. Their influence on the motion was

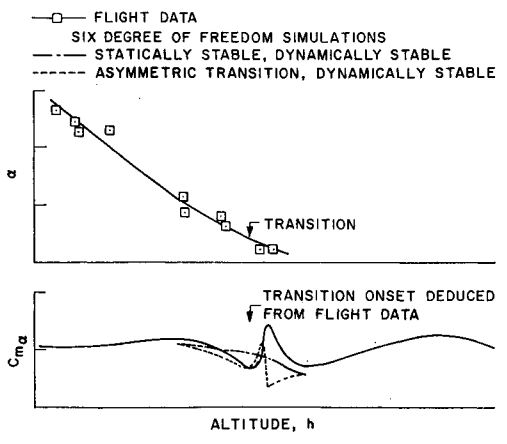

Fig. 12 Flight history of α and $C_{m\alpha}$.

established from six-degree-of-freedom simulations, which indicate that as the transition front comes on the aft vehicle surface, the statically destabilizing influences cause α to diverge. As the front traverses forward, the influence becomes stabilizing, and α decreases. Similar results are obtained when the vehicle has a period of dynamic instability. However, this latter approach does not affect the static stability of the vehicle and therefore does not account for the variations of C_{m_α} that appear in the flight data.

Figure 12 shows that there is a marked similarity between the C_{m_α}'s deduced from flight measurements with the results of six-degree-of-freedom simulations for the case with asymmetric transition. As was stated earlier, no attempt was made to scale the ground-test results to flight; consequently, quantitative agreement was not expected.

Since the incremental loads due to asymmetric transition are a manifestation of the changes in the induced pressure and shear forces on a vehicle, in principle, one should be able to predict them, provided the shape of the transition front is known. This, of course, presupposes that a viscous analytic technique exists which a) can predict the flow about a body at angle of attack and b) permits proper evaluation of the viscous-induced effects in laminar-transitional-turbulent flows, an extremely difficult requirement. The complications that arise in predicting the local properties and the forces and moments on a body when differential ablation (blowing) is present have been examined in Ref. 13 and have been attributed to the inadequacies of the weak viscous interaction models that are typically employed.

In the present study the influence of asymmetric boundary-layer transition on only the static derivatives were explored. This is not to say that the dynamic influences should be ignored. Due to the oscillatory motion of re-entry vehicles, the dynamic coupling of the static characteristics with the heat shield thermal time lag must be considered in analyzing the total problem.

Conclusions

The results of this investigation indicate that mass transfer and asymmetric transition strongly influence the motion of a slender re-entry vehicles. The angle-of-attack divergence that is normally encountered in the transitional altitude regime can be attributed in whole or in part to the static forces and moments due to the asymmetries of transition, and mass addition serves to amplify these forces and moments. At the onset of transition on the aft frustum a strong statically destabilizing force exists, for ablating vehicles with transition forward on the leeward side. As this front moves forward on the vehicle, the magnitude of the destabilizing influence diminishes, and when it reaches the vicinity of the vehicle's center of gravity, the force becomes statically stabilizing. Application of the ground test results to flight vehicles shows that a momentary angle of attack divergence can occur similar to that achieved by dynamic instabilities. In addition, the effects of asymmetric transition on the static stability cause a variation of the pitching moment coefficient slope with altitude similar to that measured in flight so that a direct cause and effect relationship was established.

References

[1] Martellucci, A., Marshall, L. A., and Kent, R. W., "Application of Ground Test Facilities to Augment Flight Data Evaluation," TIS 69SD228, Feb. 1969, General Electric, Philadelphia, Pa.

[2] Ericson, L. E., "Effect of Boundary Layer Transition on Vehicle Dynamics," *Journal of Spacecraft and Rockets*, Vol. 6, No. 12, Dec. 1969, pp. 1404–1409.

[3] *AVCO REST Sem. Annual Report Vol. II Aerophysics*, BSD TR 67-37, Feb. 1967, Wilmington, Mass.

[4] Studerus, C. J. and Dienna, E. A., "Viscous Interaction Zero Angle of Attack Drag (VIZAAD) Program," TIS 64SD292, Nov. 1964, General Electric, Philadelphia, Pa.

[5] Lees, L., "Laminar Heat Transfer Over Blunt-nosed Bodies at Hypersonic Flight Speeds," *Jet Propulsion*, April, 1956.

[6] Walker, G. K., "Turbulent Boundary Layers with Mass Addition," RSD TFM 021, Nov. 1963, General Electric, Philadelphia, Pa.

[7] Studerus, C. J. and Dienna, E. A., "Sphere Cone Angle of Attack (SCAAT) Program," Document 63SD-744, Dec. 1964, General Electric, Philadelphia, Pa.

[8] DiCristina, V., "Three-Dimensional Laminar Boundary Layer Transition on a Sharp 8° Cone at Mach No. 10," AIAA Paper 69-12, New York, Jan. 1969.

[9] Stetson, K. F. and Rushton, G. H., "Shock Tunnel Investigation of Boundary Layer Transition at $M = 5.5$," *AIAA Journal*, Vol. 5, No. 5, May 1967, pp. 899–906.

[10] DeCarlo, J. et al., "Mach 5 to 12 Inlet Development Program, Phase I—Data Report," Fairchild Hiller Report 2817-29-1, 1963, Farmingdale, N.Y.

[11] McCauley, W. D., Saydah, A., and Bueche, J., "The Effect of Controlled Three-Dimensional Roughness on Hypersonic Laminary Boundary Layer Transition," AIAA Paper 66-26, New York, Jan 1966.

[12] Martellucci, A., "Asymmetric Transition Effects on the Static Stability and Motion History of a Slender Vehicle," Document 70SD451, Jan. 1970, General Electric, Philadelphia, Pa.; also SAMSO TR-70:141.

[13] Martellucci, A., Neff, R. S., and Rittenhouse, C., "Mass Addition Effects on Vehicle Forces and Moments—Comparison Between Theory and Experiment," Document 69SD934, Sept. 1969, General Electric, Philadelphia, Pa.; also SAMSO TR 69-384